Experimental and numerical investigation on thermal and hydraulic performance of semiwavy minichannels using water–ethylene glycol-based nanofluids

P. V. R. Nanda Kishore[1] · S. Venkatachalapathy[1] · Vuppula Santhosh Reddy[1]

Abstract

A thermohydraulic performance investigation is performed on a minichannel heat sink with alternating straight and sinusoidal (semiwavy) profiles for different channel amplitudes (0.2, 0.4 and 0.6 mm). The study throws light on the performance of variable area minichannel heat sink combined with wall waviness. The effect of nanofluids as coolants for these channels is also investigated. Water–ethylene glycol, 0.4 and 1% alumina nanofluids are used as coolants. The performance enhancement coefficient is also evaluated. The maximum enhancement in Nusselt number is obtained for the wave amplitude of 0.6 mm and a nanofluid concentration of 1%. It is observed that the advantage of using nanofluids diminishes considerably with an increase in the relative waviness. The performance enhancement coefficient is found to be highest for the minichannel having the wave amplitude of 0.4 mm. Further increase in amplitude leads to higher pressure drop penalty. The numerical analysis reveals the occurrence of secondary vortices which is confined to the crest and trough regions of the semiwavy walls.

Keywords Minichannel · Nanofluids · Semiwavy · Sinusoidal · Nusselt number

List of symbols

A	Area (m^2)
A_{base}	Base area (m^2)
A_h	Heat transfer area (m^2)
C_p	Specific heat capacity (J kg^{-1} K^{-1})
D_h	Hydraulic diameter (m)
E	Voltage (V)
H_{wt}	Distance from thermocouple to channel surface (m)
h_{avg}	Average heat transfer coefficient (W m^{-2} K^{-1})
k	Thermal conductivity (W m^{-1} K^{-1})
L	Channel length (m)
$\dot{m}$	Mass flow rate (kg s^{-1})
$\dot{M}$	Total rate of mass flow (kg s^{-1})
n_c	Number of minichannels
Nu	Nusselt number
Pr	Prandtl number
Re	Reynolds number
T_w	Wall temperature (°C)
T_m	Mean temperature (°C)
V_m	Mean velocity (m/s^{-1})
$\dot{V}$	Volumetric flow rate (m^3 s^{-1})
w_c	Width of minichannel (m)
w_{fin}	Fin width (m)
ρ	Density (kg m^{-3})
μ	Dynamic viscosity (kg m^{-1}s^{-1})

Abbreviations

NF	Nanofluid
SWMC1	Semiwavy minichannel with wave amplitude 0.2 mm
SWMC2	Semiwavy minichannel with wave amplitude 0.4 mm
SWMC3	Semiwavy minichannel with wave amplitude 0.6 mm

✉ P. V. R. Nanda Kishore
    nandakishore6626@gmail.com

[1] Department of Mechanical Engineering, National Institute of Technology, Trichy, India

Introduction

Miniature channels, viz. mini-/microchannels, have been employed as effective heat dissipation devices when compared to conventional channels. Although they have superior heat transfer characteristics, the performance is constrained by high pumping power requirements. In order to ensure better performance, many methods like flow disruption, use of linear vortex generators [1], curvilinear geometries [2,

3], helical inserts, twisted tapes [4], etc. have been studied by researchers. Also, low thermal conductivity of working fluids is a stumbling block in the development of high-performance heat removal devices. This led to the use of nanofluids which are synthesized by suspending nanoparticles in some base fluids, viz. water, kerosene, ethylene/propylene glycol, etc. [5]. Vivek Kumar & Jahar Sarkar [6] conducted experimental and numerical studies in which they examined pressure drop and heat transfer characteristics in the laminar zone of a minichannel utilizing Al_2O_3–TiO_2 hybrid nanofluids.

Gong et al. [7] used wavy channels in two configurations of microchannels: one where the crests and troughs directly face one other and the other where they faced alternately with each other and the latter exhibiting higher heat transfer performance. The heat transport properties of alumina–water nanofluids across a rectangular minichannel were studied using experiments and numerical simulations by Saeed et al. [7]. Effects of fin spacing were also studied, and it was revealed that the lesser the fin spacing, the better was the heat transfer performance. The authors observed a significant increase in the heat transfer coefficient while using nanofluids. Alumina/titanium dioxide–water nanofluids were used in the numerical studies on micro- and minichannels by Ambreen et al. [8]. Single-phase, discrete phase and Eulerian–Eulerian models were compared, and it was found that all the models gave accurate hydrodynamic results for thermally less conductive fluids. In the case of high-thermal-conductivity nanofluids, single-phase models underpredict the heat transfer coefficient (HTC), whereas Eulerian–Eulerian models overpredicted the HTC results. A microscale minichannel with a backward facing step was numerically modeled by Mohamad and Gabriella [9] with two different nanofluids, viz. alumina and titanium dioxide–water. It was observed that the regions with higher-temperature gradients exhibited larger recirculation. Abhijit et al. [10] performed a conjugate heat transfer analysis through a wavy minichannel in the laminar flow regime. The authors found an underprediction in Nusselt number when the effect of wall thickness had been ignored. Leela et al. [11] performed experimental analysis on a novel minichannel sink with dual inlet and outlet plenums. The authors found a 60% reduction in the substrate temperature owing to better coolant distribution. In the experimental work by Balaji et al. [12], hybrid nanofluids comprising MWCNT and graphene were used as coolant in a microchannel. The authors confirmed that the nanofluid can effectively facilitate better removal when compared with water. Using three different heat inputs of 25, 35 and 45 W, Sajid et al.[13] examined the TiO_2 nanofluid's heat transfer capability in the laminar zone using three wavy channel designs. The investigated nanofluid concentrations were 0.006, 0.008, 0.01 and 0.012% by volume, and the outcomes were compared with those obtained using pure water.

In comparison with its width, it was discovered that the Nusselt number is highly dependent on the channel wavelength.

Nivedita et al. [14] used spiral channels and studied the development of Dean vortices for different aspect ratios. Sui et al. [2] conducted a numerical investigation in wavy microchannels and found the presence of Dean vortices which resulted in higher heat transfer rates. They also concluded that faster heat transfer rates were achieved when the amplitude-to-wavelength ratio is increased. In the heat transfer performance study by Lin et al. [15] using wavy microchannels, the authors discovered the influence of secondary vortices in enhancing fluid mixing. Impact of the channel aspect ratio was also looked into. The transfer of heat through a hexagonal microchannel heat sink was numerically investigated by Alfaryjat et al. [14]. The study employed various H_2O-based nanofluid coolants, viz. alumina, copper oxide, silicon dioxide and zinc oxide. The study evaluated the heat transfer performance of these coolants with that of the base fluid. Alumina water nanofluid exhibited the highest heat transfer performance. Heat transfer studies on single-/double-layer wavy microchannels were carried out by Gongnan et al. [16] with water as coolant. Based on the evaluation of both thermal and hydraulic capabilities, double-layer channels demonstrated superior performance. Aliabadi et al. [17] conducted numerical study on two cases of wavy minichannel fluid flow, viz. co-current and countercurrent, for different amplitudes and wavelengths in the laminar flow regime. They found an average reduction of 5.5 K for counterflow regime. Hussain et al. [18] studied different configurations of dual flow channels for different fin thickness and compared the performances with a straight minichannel.

The thermohydraulic performance of water-based alumina nanofluids was numerically investigated by Seyed et al. [19] in a triangular minichannel. In comparison with water, the authors discovered that using nanofluids resulted in a minor pressure drop penalty. Ping et al. [18] used alumina–water nanofluid to study the heat transfer performance in a microchannel with dimpled/protrusion surfaces. The authors found notable changes in the flow patterns as the concentration of nanofluid increased. Ribs in microchannels were employed by Karthikeyan et al. [19] to study the heat transfer performance. They came to the conclusion that rib width significantly contributed to the increased heat transfer rates. Nanda Kishore et al. [20] used hybrid nanofluids (alumina, copper oxide–DI water) in wavy and a novel semiwavy minichannel with rectangular cross section and found better mixing of fluid in the wavy channel. The cooling performances of different sinusoidal minichannel heat sinks were studied by Aliabadi et al. [3]. The effect of wave amplitude and wavelength on heat transfer performance were also studied. Wang et al. [21] conducted a 3D conjugate heat transfer analysis of a ribbed counterflow minichannel heat sink with slots incorporated on the ribbed surfaces. Water was used as

a coolant and the authors found that slots helped in periodic rupture and redevelopment of boundary layer leading to better heat transfer. The performance of a triangular minichannel with wavy vortex generator was investigated by Elham and Faramarz [22] using alumina–water nanofluid.

In this research work, numerical and experimental studies are conducted in semiwavy minichannels of three different relative waviness and the thermohydraulic performance is compared with a straight rectangular channel. Also, the performance of the channels are compared for two coolants, viz. water–ethylene glycol mixture (60:40) and alumina nanofluid (0.4 and 1% vol. concentration). The geometry selected in the study was introduced in the previous experimental work by the same authors [20]; however, the comparative performance of the channel with different waviness has not been studied so far. The comprehensive thermohydraulic performance is ascertained using performance enhancement coefficient. The comparative performances of working fluids are discussed for different cases.

The influence of convergent–divergent zones in minichannels on heat transfer enhancement has well been reported in the literature. The basic mechanism for this enhancement has been attributed to thermal boundary layer disruption and flow separation. Heat transfer enhancement in wavy profile channels also has been found to be higher compared to their straight counterparts owing to thinning of hydrodynamic and thermal boundary layers. However, heat transfer studies on the comparative performance of the convergent–divergent wavy channels with different waviness have not been studied so far. The geometry selected in the study was introduced in the previous experimental work by the same authors [20]. In this research work, numerical and experimental studies are conducted in semiwavy minichannels of three different relative waviness and the thermohydraulic performance is compared with a straight rectangular channel. Also, the performance of the channels is compared for two coolants, viz. water–ethylene glycol mixture (60:40) and alumina nanofluid (0.4 and 1% vol. concentration). The comprehensive thermohydraulic performance is ascertained using performance enhancement coefficient. The comparative performances of working fluids are discussed for different cases.

Materials and methods

The coolants used in this study are water–ethylene glycol (60:40), 0.4 and 1% alumina nanofluids. Alumina nanoparticles and ethylene glycol are procured from SRL India Pvt. ltd. The base fluid for both nanofluids is a combination of water and ethylene glycol. Using SEM, the alumina nanoparticles' surface morphology is discovered to be spherical with a mean diameter of about 40 nm. The SEM image of the nanoparticles is shown in Fig. 1. The

XRD analysis of the alumina nanoparticles employed in this investigation (which was covered in the work done by the same authors [20]), ensures that there are no contaminants present.

It takes two steps to prepare the nanofluid. For two hours, a magnetic stirrer is used to mix the calculated amount of alumina according to Eq. (1) into the base fluid, which is a 60:40 ratio of water to ethylene glycol. Following this, the mixture is sonicated using a probe sonicator (25 kHZ, 750 W, Nabarupayan make) for 90 min in order to prevent agglomeration of nanoparticles and to achieve effective dispersion. No surfactants are used as it causes foaming issues, which may eventually lead to reduced heat transfer.

$$\text{Volume concentration, } \phi = \frac{m_{Al_2O_3}}{\rho_{Al_2O_3}} \bigg/ \frac{m_{Al_2O_3}}{\rho_{Al_2O_3}} + \frac{m_{water-EG}}{\rho_{water-EG}}$$

(1)

Stability evaluation

The stability of the nanofluid is evaluated in this work using the zeta potential test. Using Zeta sizer Nano ZS, the zeta potential of 1% alumina nanofluid is found to be 44.7 mV as shown in Fig. 2. The potential difference between the liquid layer affixed to the nanoparticles and the dispersion medium is known as the zeta potential. Particles are said to be at the isoelectric point if the zeta potential is approximately zero. Particle dispersion begins when the zeta potential of the particles is less than 30 mV. A zeta potential between 30 and 60 mV indicates good stability [23]. Accordingly, the working fluid used in this study can be classified as a stable one.
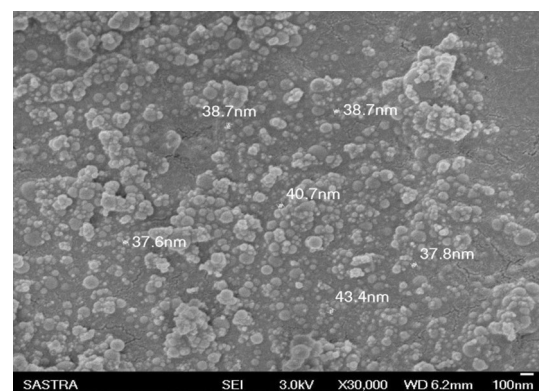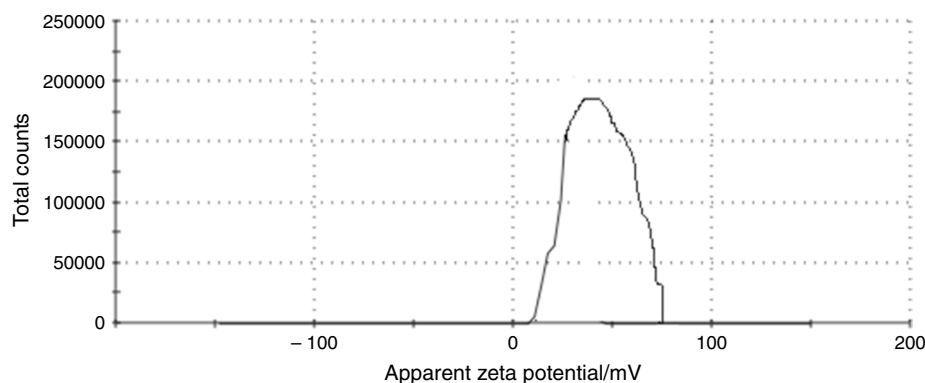

Fig. 1 SEM image of Al$_2$O$_3$ nanoparticles

Fig. 2 Zetapotential of 1% alumina nanofluid

Experimental methods

Experimental setup

Figure 3 illustrates the schematic sketch of the experimental setup, which comprises three sections: an acrylic cover, an intermediate PEEK housing and a wooden bottom housing. The intermediate plate includes inlet and outlet plenums along with a slot for fixing the minichannel heat sink block. The heater block is centrally placed in the bottom housing. A symmetric design is adopted for the inlet and outlet plenums. Both the plenums are provided with a deep and shallow zone in succession to ensure smooth, uniform flow of coolant as it enters the channel. For achieving maximum contact between the heater block and minichannel base, thermal grease is used. The margins of the minichannel are sealed with silicone sealant once it has been inserted into the intermediate plate. Fiber glass insulation is placed around the heater to minimize heat losses. Slots are provided in the intermediate housing for inserting thermocouples to measure wall temperatures at specified locations in the minichannel heat sink. There are pressure tapings available for the minichannel sink in both upstream and downstream sections. The heat input is provided by a 400W cartridge heater. A DC power source

(Seleicon make) supplies the required power input to the cartridge heater.

Procedure

As depicted in Figs. 3–5, a peristaltic pump (Ravel Hiteks Pvt. limited) is used to pump the coolant from constant temperature bath (Lark innovative) to the minichannel sink. The coolant returns to the constant temperature bath after receiving heat from the minichannel heat sink. At the bottom of the minichannel block, a heat flux of 83 kW m^{-2} is applied, and a constant inlet temperature of 293 K is maintained for the coolant. A pulse dampener is included in the circuit to dampen the flow fluctuations from the peristaltic pump. T-type thermocouples are used to measure the temperatures of wall, coolant inlet and outlet. A data logger (Keysight Technologies) is used to record all the temperatures. Five thermocouples are positioned 5 mm below the channel surface and spaced 10 mm apart in order to measure the temperature of the channel wall. The difference between the pressure at the inflow and outflow is measured using a pressure transducer (supplied by ABB).

Fig. 3 Schematic of minichannel assembly
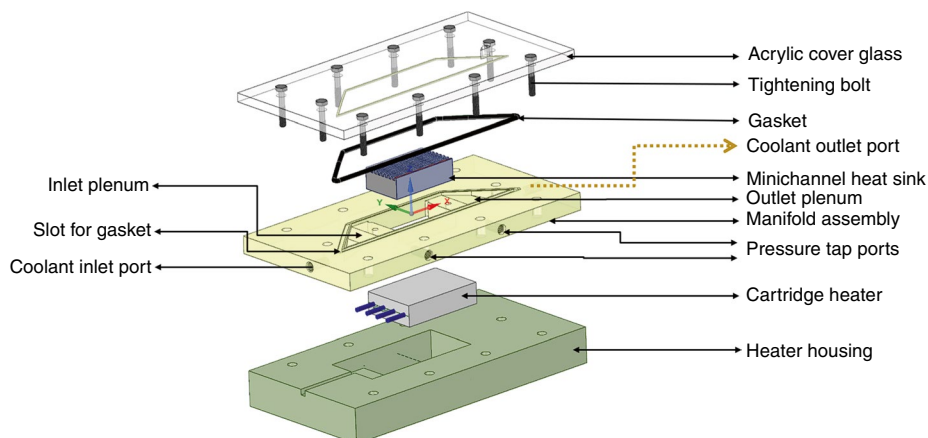
Case description

Three different configurations of semiwavy minichannels (SWMC) having different amplitudes) are fabricated using CNC milling process on blocks of same foot print area of 50×30 mm with a thickness of 10 mm. In the SWMC, the channel walls on the left and right have an alternating straight and wavy profile. Also, each straight wall on either side has an opposing wavy wall and vice versa, thus forming regular converging and diverging sections. In all the

channels, sinusoidal profile ($y = a.\sin 2\pi x/\lambda$, where a is the amplitude and λ the wavelength) is used for developing the wavy wall. All minichannels have an identical hydraulic diameter, number of channels and channel height. Due to its high thermal conductivity, copper block is used to fabricate the minichannels. The geometrical parameters of all the channels used in the study are shown in Table 1. The photograph and schematic of the minichannel are depicted in Fig. 6a and b.
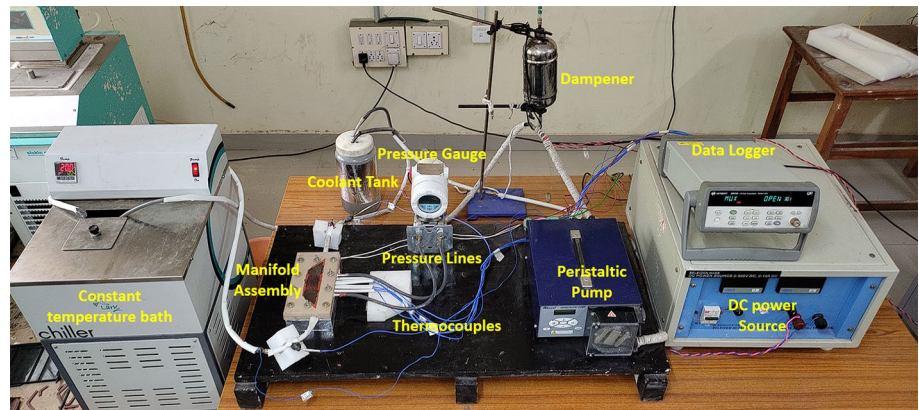

Fig. 4 Photograph of experimental setup

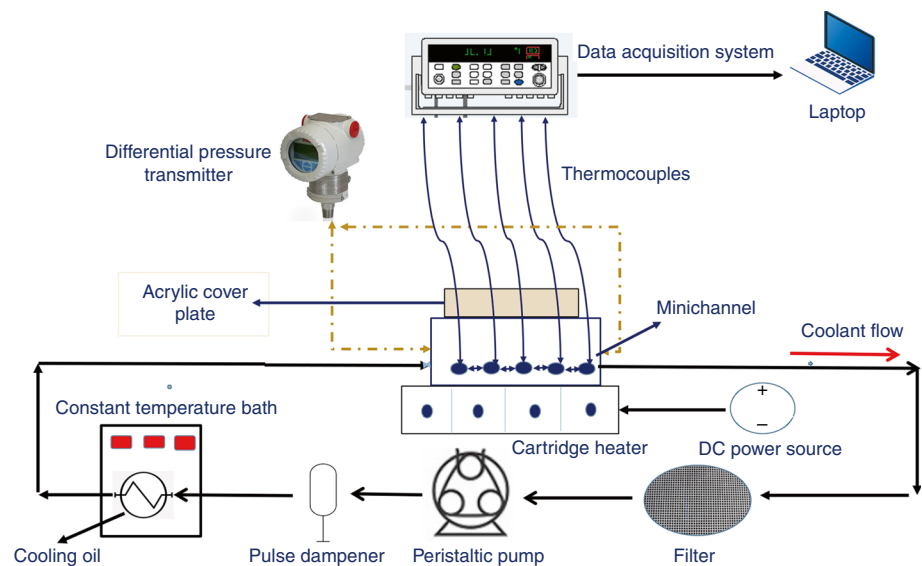Fig. 5 Schematic of the experimental setup

Table 1 Geometrical parameters of the minichannels

Geometry of minichannels	Channel height/mm	Channel width/mm		Channel length/mm	Wavelength/ mm	Amplitude/mm	Number of channels	Heat transfer area/ mm^2
		Inlet	Outlet					
SWMC1	2	2	2	50	10	0.2	8	2403.01
SWMC2	2	2	2	50	10	0.4	8	2412.30
SWMC3	2	2	2	50	10	0.6	8	2427.44

Fig. 6 a Photograph of SWMC3
b Schematic of SWMC3

(a)

(b)

(All dimensions are in mm)
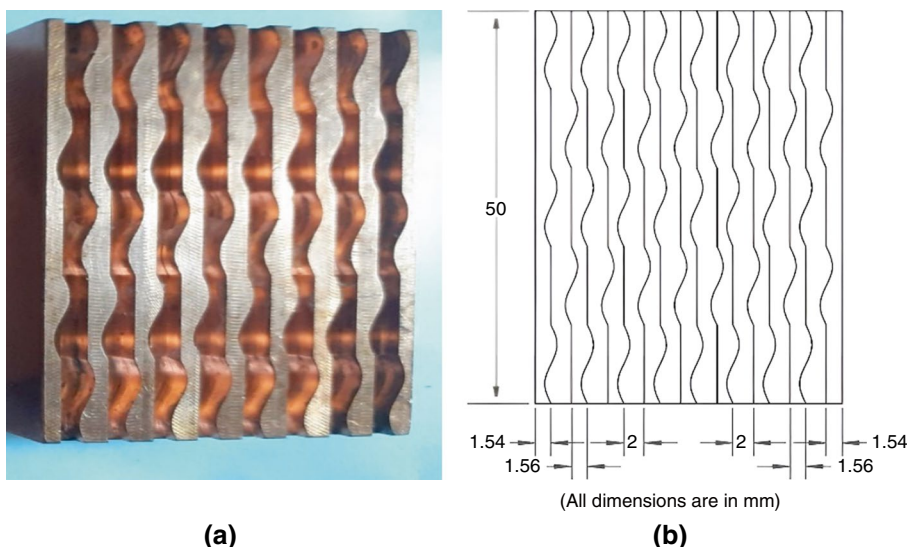
Experimental data reduction

Heat applied,

$$Q_{\text{applied}} = \text{EI} \tag{2}$$

where the voltage is represented by E and the current by I.

From the energy balance, the rate of heat absorption by the coolant,

$$Q_{\text{actual}} = \dot{M}C_{\text{p}}\left(T_{\text{outlet}} - T_{\text{inlet}}\right) \tag{3}$$

M is the total working fluid rate of mass flow and cp is the specific heat.

Volumetric flow rate of the fluid in operation

$$\dot{V} = n_{\text{c}}A_{\text{c}}V_{\text{m}} \tag{4}$$

where A_{c} is the area of a single channel's cross section, V_{m} is the average flow velocity and n_c is the number of channels.

Total mass flow rate of the working fluid,

$$\dot{M} = n_{\text{c}}\dot{m} \tag{5}$$

where $\dot{m}$ is the coolant mass flow rate through a single channel.

Reynolds number,

$$\text{Re} = \rho_{\text{fluid}}V_{\text{m}}D_{\text{h}}/\mu_{\text{fluid}} \tag{6}$$

where the fluid mean velocity is represented by V_{m}, hydraulic diameter by D_h and fluid density by ρ_{fluid}. Due to measurement constraints, the wall temperature cannot be directly obtained. So it is evaluated by using temperature data 5 mm underneath the top surface (ith location-T_{tc}) of the heat sink along the midplane by assuming one-dimensional heat conduction.

Temperature of the wall next to the channel surface's ith position [24],

$$T_{\text{wi}} = T_{\text{tc}} - \left(Q_{\text{act}}H_{\text{wt}}/k_{\text{cu}}A_{\text{base}}\right) \tag{7}$$

T_{tc} is the thermocouple location at the channel surface that corresponds to ith location, and H_{wt} is the distance measured between the thermocouple and the channel surface.

Base area of heat sink,

$$A_{\text{base}} = n_{\text{c}}L\left(w_{\text{c}} + w_{\text{fin}}\right) \tag{8}$$

where w_c and w_{fin} are the width of the channel and fin, respectively, and L is the channel length.

Next, the channel base's average wall temperature is calculated as

$$T_{\text{w}} = \sum_{1}^{5} T_{\text{wi}}/5 \tag{9}$$

The average convective heat transfer coefficient is found by applying Newton's equation of cooling.

$$h_{\text{avg}} = Q_{\text{act}}/A_{\text{h}}\left(T_{\text{w}} - T_{\text{m}}\right) \tag{10}$$

The heat transfer area is represented by A_{h}, and the mean coolant temperature, or T_{m}, is determined by averaging the temperatures at the inlet and outlet.

At the mean temperature, the coolant's thermophysical characteristics are computed.

Average Nusselt number,

$$\text{Nu}_{\text{avg}} = h_{\text{avg}}D_{\text{h}}/k_{\text{fluid}} \tag{11}$$

The average friction factor,

$$f = 2\Delta p D_\mathrm{h} / L\rho V_\mathrm{m}^2 \qquad (12)$$

where Δp is the pressure drop measured between the inlet and outlet of the heat sink and ρ is the density of the fluid.

Performance evaluation coefficient (PEC) for nanofluid is calculated as [25, 26]

$$\eta_\mathrm{nf} = \left(Nu_\mathrm{nf} / Nu_\mathrm{water}\right) \Big/ \left(f_\mathrm{nf} / f_\mathrm{water}\right)^{1/3} \qquad (13)$$

Uncertainty analysis

To evaluate the uncertainties in the salient parameters, the following approach (Kline and McClintock) has been used:

$$\frac{\Delta Nu}{Nu} = \sqrt{\left(\frac{\Delta h}{h}\right)^2 + \left(\frac{\Delta D_\mathrm{h}}{D_\mathrm{h}}\right)^2 + \left(\frac{\Delta k}{k}\right)^2} \qquad (14)$$

$$\frac{\Delta f}{f} = \sqrt{\left(\frac{\Delta D_\mathrm{h}}{D_\mathrm{h}}\right)^2 + \left(\frac{\Delta(\Delta P)}{\Delta P}\right)^2 + \left(\frac{\Delta L}{L}\right)^2 + \left(\frac{\Delta \rho}{\rho}\right)^2 + \left(\frac{2\Delta V_\mathrm{m}}{V_\mathrm{m}}\right)^2} \qquad (15)$$

Accordingly, the uncertainties in Nusselt number and friction factor are estimated as ± 6.71 and $\pm 5.66\%$, respectively.

Numerical implementations

Computational model and governing equations

The computational model of the various minichannel cases considered for the study is depicted in Fig. 7a–c. Structured hexahedral mesh is generated in ANSYS ICEM 19.2. The meshing strategy ensures one-to-one matching of grid points of solid and fluid zones to ensure conformity. As shown in Fig. 8, only one channel is chosen as the computational domain for simulation in order to reduce computing time and expense.

Assumptions

To simplify the problems, several assumptions have been adopted in accordance with [7, 17, 27, 28].

Single-phase, three-dimensional conjugate heat transfer under steady-state conditions is assumed.

Flow is laminar and no-slip conditions are assumed at the walls.
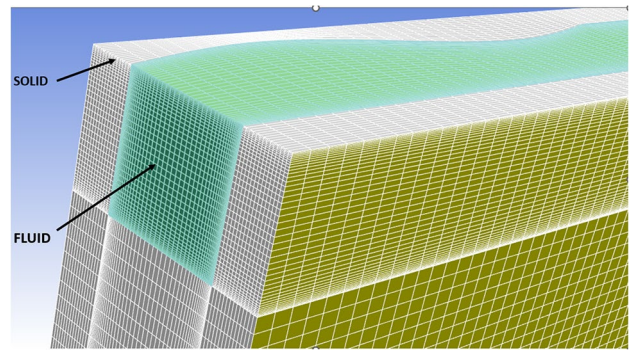
Coolant used is incompressible.

Fig. 8 Combined fluid and solid mesh domains

With respect to mean fluid temperature, nanofluid is represented as a single-phase fluid with constant characteristics.

All the surfaces, apart from the bottom face, which receives heat, are assumed to be adiabatic.

Radiation effects are neglected.

The following are the pertinent governing equations for the given problem.

Continuity equation:

$$\frac{\partial u}{\partial x} + \frac{\partial v}{\partial x} + \frac{\partial w}{\partial x} = 0 \qquad (16)$$
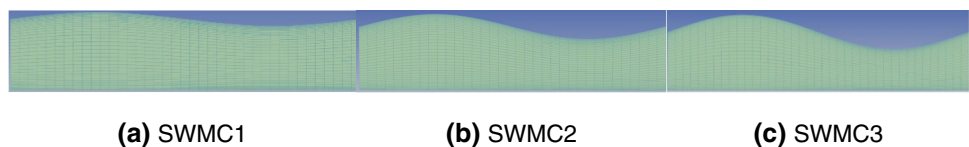
Momentum equation:

$$\rho_\mathrm{f}\left(u\frac{\partial u}{\partial x} + v\frac{\partial u}{\partial y} + w\frac{\partial u}{\partial z}\right) = -\frac{\partial p}{\partial x} + \mu_\mathrm{f}\left(\frac{\partial^2 u}{\partial x^2} + \frac{\partial^2 u}{\partial y^2} + \frac{\partial^2 u}{\partial z^2}\right) \qquad (17)$$

$$\rho_\mathrm{f}\left(u\frac{\partial v}{\partial x} + v\frac{\partial v}{\partial y} + w\frac{\partial v}{\partial z}\right) = -\frac{\partial p}{\partial y} + \mu_\mathrm{f}\left(\frac{\partial^2 v}{\partial x^2} + \frac{\partial^2 v}{\partial y^2} + \frac{\partial^2 v}{\partial z^2}\right) \qquad (18)$$

$$\rho_\mathrm{f}\left(u\frac{\partial w}{\partial x} + v\frac{\partial w}{\partial y} + w\frac{\partial w}{\partial z}\right) = -\frac{\partial p}{\partial z} + \mu_\mathrm{f}\left(\frac{\partial^2 w}{\partial x^2} + \frac{\partial^2 w}{\partial y^2} + \frac{\partial^2 w}{\partial z^2}\right) \qquad (19)$$

Energy equation for solid zone:

$$k_\mathrm{s}\left(\frac{\partial^2 T_\mathrm{s}}{\partial x^2} + \frac{\partial^2 T_\mathrm{s}}{\partial y^2} + \frac{\partial^2 T_\mathrm{s}}{\partial z^2}\right) = 0 \qquad (20)$$

Fig. 7 Mesh details—top view of SWMC1 (**a**), SWMC2 (**b**) and SWMC3 (**c**)

(a) SWMC1   **(b)** SWMC2   **(c)** SWMC3

Energy equation for fluid zone:

$$\rho_f C_{pf}\left(u\frac{\partial T_f}{\partial x} + v\frac{\partial T_f}{\partial y} + w\frac{\partial T_f}{\partial z}\right) = k_s\left(\frac{\partial^2 T_s}{\partial x^2} + \frac{\partial^2 T_s}{\partial y^2} + \frac{\partial^2 T_s}{\partial z^2}\right) \tag{21}$$

where u, v and w denote the velocity components in the x, y and z directions, respectively, T and p indicate the fluid temperature and pressure, respectively, and ρ, μ, k and cp represents density, dynamic viscosity, thermal conductivity and specific heat of the fluid, respectively. T_s and K_s denotes the solid temperature and solid thermal conductivity, respectively.

The governing equations for the conjugate heat transfer problem are solved using ANSYS FLUENT 19.2 adopting the finite volume method. For the pressure term, discretization scheme used is standard. The semi-implicit approach is used to solve the pressure–velocity coupling [25].

Second order upwind differencing approach for the energy and momentum equations has been adopted. Double precision method is used, as the scales of the domain are small. The inlet conditions are used to initialize the flow field and the convergence threshold for the mass, momentum and energy equations is maintained at a residual of 10^{-7}.

Boundary conditions

Inlet

Velocity boundary condition is prescribed at the inlet and all experiments are conducted for an inlet temperature of 298 K.

$$V = V_{inlet} \tag{22}$$

Bottom surface

Constant heat flux boundary condition is applied at the channel bottom surface.[17, 19, 29].

$$q = -k_{cu}\frac{\partial T}{\partial n} \tag{23}$$

Solid–fluid interface

$$-k_{fluid}\frac{\partial T}{\partial n} = -k_{solid}\frac{\partial T}{\partial n} \tag{24}$$

Outlet

Pressure outlet boundary condition is prescribed. Flow outlet pressure has been assigned as atmospheric pressure.

Table 2 Thermophysical properties of materials used

Property	Water–EG (mixture) at 30 °C [30]	Al$_2$O$_3$
Density kg m^{-3}	1031	3880
Specific heat J kg^{-1} K^{-1}	3735	729
Thermal conductivity W m^{-1}K^{-1}	0.412	40

Table 3 Grid Independency

Case	Number of elements	Average Nusselt number	% Error
1	962,355	10.85	–
2	1,051,231	11.17	2.94
3	1,290,384	11.35	1.61
4	1,380,710	11.39	0.35

Sidewalls

Symmetry boundary condition is used.

Thermophysical properties

The various thermophysical properties of materials used are shown in Table 2. The thermal conductivity and viscosity of 0.4 and 1% alumina nanofluid (basefluid—60:40 water–ethylene glycol) are adapted from the work by Chiam et al. [31]. The thermophysical properties are selected at the mean coolant temperature.

Grid independent study

Table 3 illustrates the mesh independency study conducted for the semiwavy channel, SWMC3 for a Reynolds number of 360. As observed from the table, the variation in average Nusselt number between case 3 and 4 is very nominal (less than 0.5%), and hence, the number of elements selected for all the geometries is 1,290,384.

Results and discussion

Nusselt number

The reliability of the experimental setup is first checked by circulating water through the minichannel array and simultaneously supplying a constant heat input of 125 W. The detailed energy balance is discussed in the previous

work by the same authors [20] using the same experimental setup. Accordingly, a mean heat loss of 5.38% was observed suggesting the satisfactory reliability of the setup. Due to paucity of results for the semiwavy minichannels used in this study, the validation has been performed for a straight rectangular channel with identical hydraulic diameter using water as coolant. The average Nusselt numbers based on numerical and experimental results are validated with the Grigull and Tratz correlation [32] for laminar flow under constant heat flux condition.

$$\text{Nu} = 4.364 + \frac{0.0668\left(\text{Re}D_{\text{h}}\text{Pr}/L\right)}{1 + 0.4\left(\text{Re}D_{\text{h}}\text{Pr}/L\right)^{2/3}} \qquad (25)$$

The validation plots are shown in Fig. 9 which clearly indicates a mean deviation of 2.4 and 2.54%, respectively, for the experimental and numerical Nusselt numbers when compared to the correlation mentioned above. This shows that the experimental setup used in this study and the numerical code implemented can be further used to study the heat transfer performance of the semiwavy minichannels.

Figure 10 compares the experimental thermal performance of SWMC3 (semiwavy channel with wave amplitude 0.6) with the numerical simulation for different working fluids, viz. water–ethylene glycol mixture, 0.4 and 1% alumina nanofluids. In the range of Reynolds numbers (90–540), the mean discrepancy between the experimental and numerical results with water–ethylene glycol is 6.1%, and the average variances with 0.4 and 1% nanofluid are 7 and 10.5%,
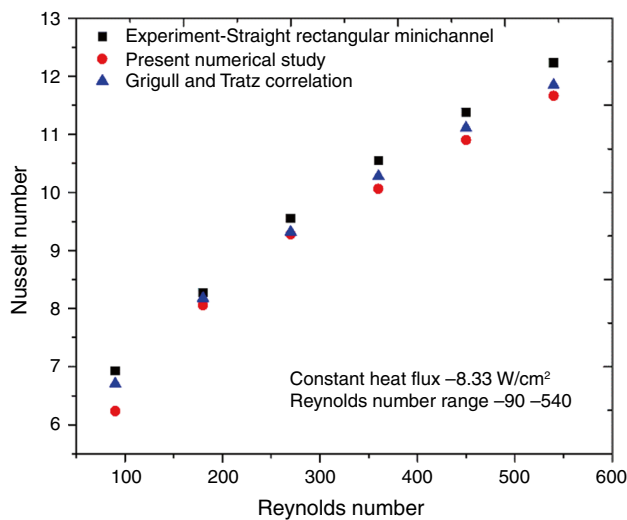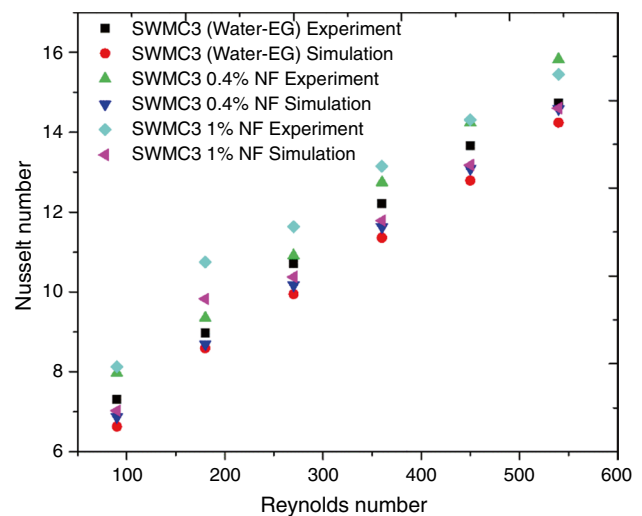

Fig. 10 Comparison of experimental and numerical results of Nusselt number for SWMC3 at different Reynolds numbers

respectively. Further, the simulations are performed for SWMC1 and SWMC2 with different Reynolds numbers with a fluid inlet temperature of 298 K (constant heat flux of 83 kW m^{-2}).

In Fig. 11, the heat transfer performance is compared numerically for all the three semiwavy minichannels with a straight rectangular channel having the same hydraulic diameter, foot print area and number of channels. As seen from the figure, when water–EG is used as the coolant,
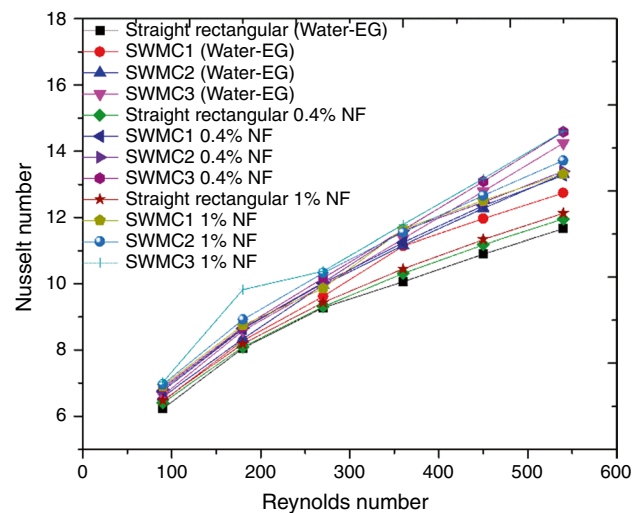

Fig. 9 Validation of experimental and numerical results with correlation

Fig. 11 Nusselt number vs Reynolds number for the different semiwavy cases

SWMC1, SWMC2 and SWMC3 exhibits a mean Nusselt number enhancement of 6.8, 9.5 and 13.74%, respectively (in the range of Re considered) when compared to straight channel. With a nanofluid concentration of 0.4%, the corresponding values are 7, 9.95 and 14.17%. The corresponding Nusselt number enhancement values for a nanofluid concentration of 1% are 7.78, 10.45 and 15%, respectively.

The semiwavy minichannels give better heat transfer enhancement compared to a straight minichannel of the same hydraulic diameter. This is due to the periodic thinning of boundary layer at regions of crest and trough, together with the regular rupture of boundary layer due to the convergent–divergent nature of the channel. Since there is a variation in wall curvature as the fluid moves along, it causes reorientation of vortices. Zones where there is a reduction in area acts as flow accelerators. Similarly, flow deceleration effect occurs at the regions of area increase. The regular repetition of the pattern contributes to heat transfer enhancement.

Figure 12 shows the streamline pattern occurring at the crest for water—ethylene glycol (a representative wave crest at $x/L = 0.5$ is considered for illustration) in a plane normal to the flow direction for the three semiwavy minichannels. It can be clearly observed that secondary vortices are found to occur at the regions of crests and troughs. As the working fluid passes through the minichannel, centrifugal forces induce pairs of counterrotating vortices. These vortices enhances the mixing between the fluid near the walls and the core fluid causing higher heat transfer [14]. As observed from Fig. 12, it is obvious that as velocity of flow increases, the swirling also increases resulting in flow distortion in the normal direction. With the increase in the velocity, the vortices move the fluid from higher-temperature wall to the core. This causes the disruption of thermal boundary layer which in turn enhances the heat transfer (Paper 280).

The streamline patterns for water–ethylene glycol working fluid at Re = 360 at three locations, viz. 2.5 mm before the crest, exactly at the crest and 2.5 mm after the crest, are depicted in Fig. 13. Secondary flow is observed only at the crest location. The design of the channel is in such a way that convergent–divergent sections are created at regular intervals along the channel, which helps in breaking of the boundary layer. Figure 14 shows the streamline pattern at a crest and the corresponding trough of SWMC3 for a Reynolds number of 360. It can be clearly understood that at the regions of crest, the channel width is at its minimum causing a converging stream. This along with the waviness can effectively rupture the boundary layer. But in the trough region, even though secondary vortices develop, due to the reduction of mean velocity, stagnation zones tend to develop, causing boundary layer growth. These results clearly show that the influence of geometry is more pronounced than

the type of working fluid at higher amplitudes, and hence, water–ethylene glycol mixture alone is sufficient to get the required heat transfer performance.

Maximum Nusselt number enhancement is observed for SWMC3 (highest amplitude) for water as well as nanofluid and this is due to two reasons: (a) strengthening of counter-rotating vortices as shown in Fig. 12 and (b) increase in the heat transfer area.

Friction factor

Due to small dimensions of the minichannel, the measurement of individual pressure drop across each channel is difficult. So, the mean pressure drop is recorded between inlet and outlet of the minichannel array and the friction factor is evaluated for each case and is depicted in Fig. 15. Since friction factor is inversely proportional to square of velocity, the average friction factor for every case in the current study exhibits an asymptotic drop with an increase in Reynolds number.

When water–EG mixture is used as working fluid, SWMC1, SWMC2 and SWMC3 exhibit an increase of 4.3, 20.27 and 46.36% in friction factor, respectively, compared to the straight rectangular channel of same hydraulic diameter. The corresponding increase with 0.5%. vol. nanofluid are 4.7, 23.21 and 49.5%, respectively. 1% vol. nanofluid exhibits a friction factor rise of 12.5, 24.24 and 61.85%, respectively, over the straight rectangular counterpart. As expected, use of nanofluids imposes an additional pressure drop penalty due to higher viscosity. With water–EG, compared to the straight rectangular channel, SWMC3 exhibits the highest friction factor increase. This is because SWMC3 has the maximum wave amplitude of 0.6 mm leading to more secondary vortices at the wave crests and troughs causing elevated pressure drop in the channel. Largest pressure drop penalty is observed for SMWC3 with 1% nanofluid. This is due to the combined effects of higher values of channel amplitude and viscosity of the working fluid.
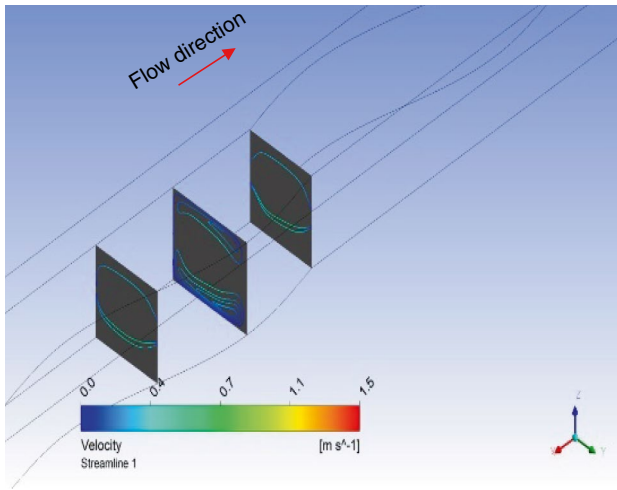
Performance enhancement coefficient

Performance enhancement coefficient (PEC) is compared for the various scenarios examined in this study for the assessment of combined thermal and hydraulic characteristics as shown in Fig. 16 A PEC value greater than one indicates superior performance compared to water–ethylene glycol. For almost all the cases in this study, PEC is greater than one; the best performance is observed for SWMC2 using nanofluids. Also, with the increase in the Reynolds number, the PEC shows a downward trend which is consistent with the findings of [27]. For SWMC3, the use of 1% alumina nanofluid does not yield better heat transfer performance due to higher pressure drop penalty.

Fig. 12 Streamlines at the location x/L = 0.5 for (**a**) SWMC1 (**b**) SWMC2 (**c**) SWMC3 (Streamlines pertain to the plane normal to the flow direction)

Re = 90   Re = 360

(a)

Re = 90   Re = 360

**(b)**

Re = 90   Re = 360

(c)
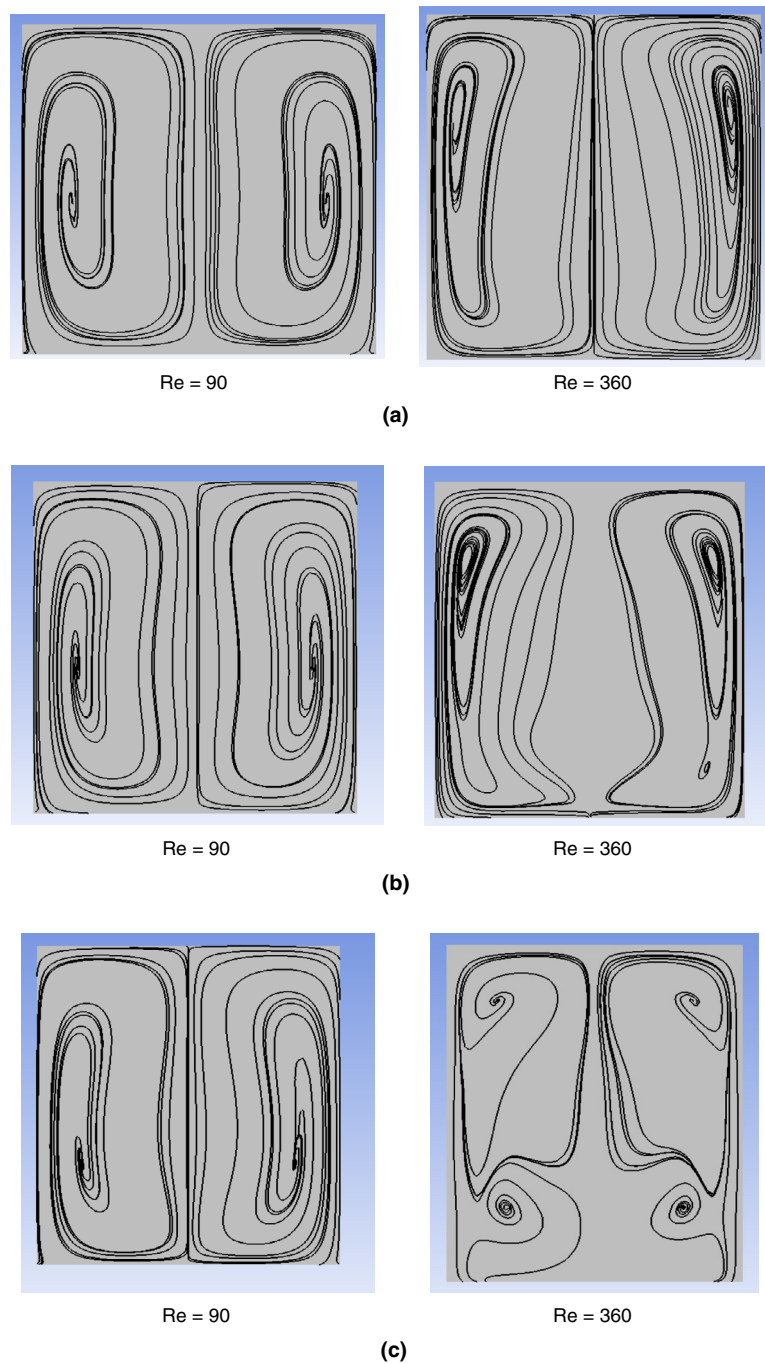
Conclusions

1. Thermohydraulic studies on the performance of semiwavy minichannels are conducted experimentally and numerically with water–ethylene glycol, 0.4 and 1% alumina nanofluids. Highest Nusselt number enhancement of 15.74% is obtained for the semiwavy minichannel of highest wave amplitude (0.6 mm) using 1% nanofluid. The corresponding friction factor increase is 61.85%.

2. In the crests and troughs of the channel, the influence of secondary vortices along with converging/diverging nature of the channel contribute to periodic rupture of the boundary layer.

3. Increasing the relative waviness does not yield better heat transfer enhancement for nanofluids.

4. The performance enhancement coefficient tends to decrease with the increase in flow rates, indicating the predominant effect of viscosity.

(a)
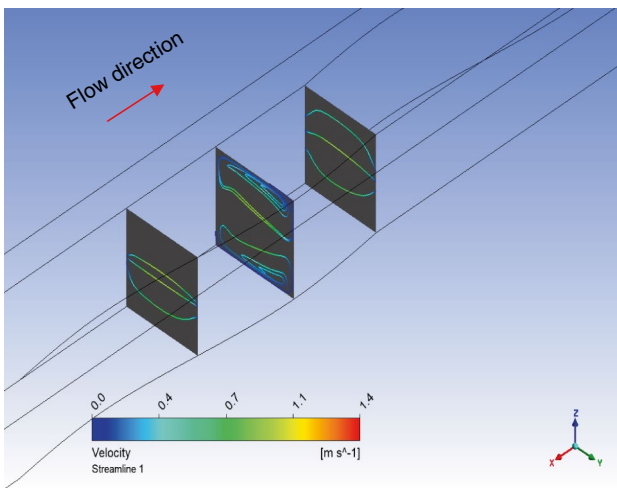
(b)
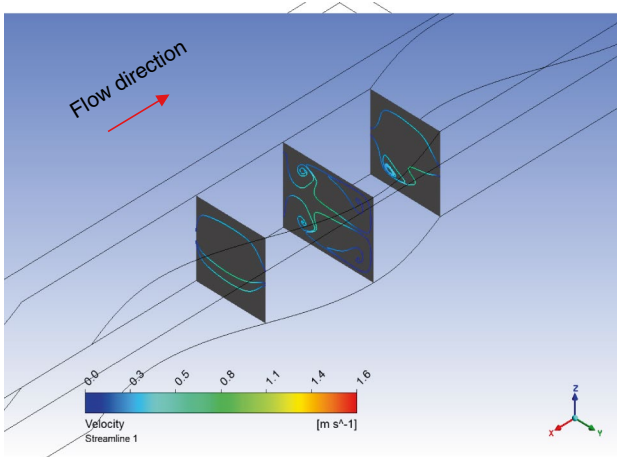
(c)

Fig. 13 Streamline patterns for (**a**) SWMC1 (**b**) SWMC2 and (**c**) SWMC3
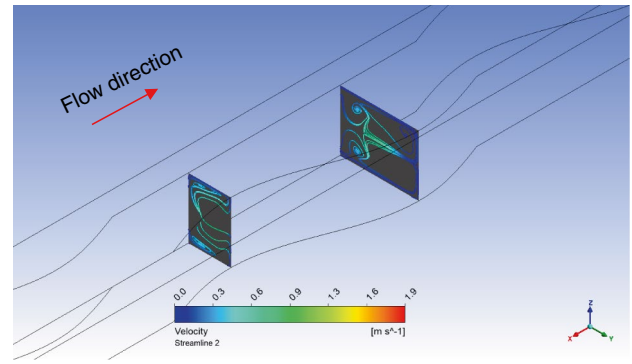

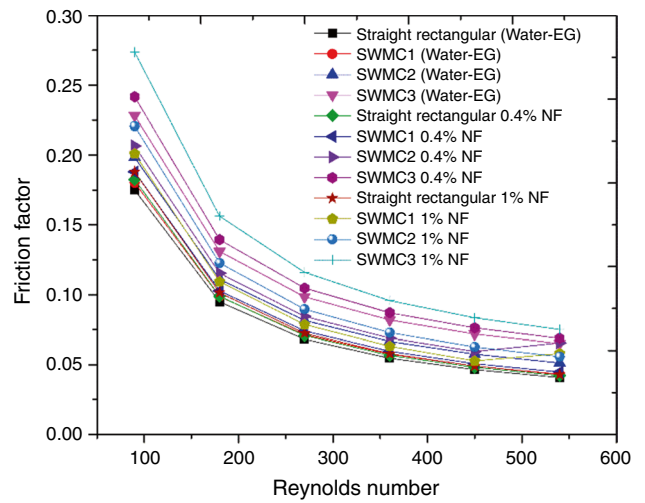**Fig. 14** Streamline patterns at crest and corresponding trough for SWMC3 (Re = 360)

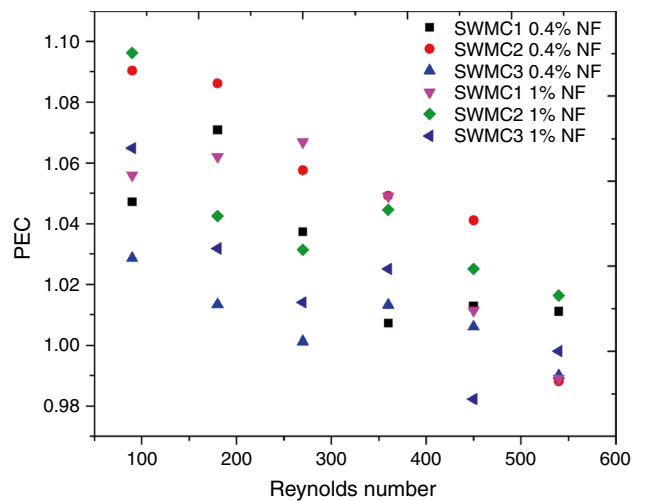**Fig. 15** Friction factor versus Reynolds number

Fig. 16 Performance enhancement coefficient versus Reynolds number

5. The results clearly indicate the dominance of geometrical parameter over the type of working fluid on the thermohydraulic performance of the semiwavy minichannels at higher amplitudes.

Author contributions Nanda Kishore P V R was involved in conceptualization, methodology, investigation, visualization, writing original draft, validation and software. S. Venkatachalapathy was responsible for methodology, resources, supervision, validation and review. Vuppula Santhosh Reddy contributed to visualization, review and editing.

References

1. Wang J, Yu K, Ye M, Wang E, Wang W, Sundén B. Effects of pin fins and vortex generators on thermal performance in a microchannel with Al_2O_3 nanofluids. Energy. 2022;15(239):122606.
2. Sui Y, Teo CJ, Lee PS, Chew YT, Shu C. Fluid flow and heat transfer in wavy microchannels. Int J Heat Mass Transf. 2010;53:2760–72.
3. Khoshvaght-Aliabadi M, Hassani SM, Mazloumi SH. Enhancement of laminar forced convection cooling in wavy heat sink with rectangular ribs and Al_2O_3/water nanofluids. Exp Therm Fluid Sci. 2017;89:199–210. https://doi.org/10.1016/j.expthermflusci.2017.08.017.
4. Maradiya C, Vadher J, Agarwal R. The heat transfer enhancement techniques and their thermal performance factor. Beni-Suef Univ J Basic Appl Sci. 2018;7:1–21. https://doi.org/10.1016/j.bjbas.2017.10.001.
5. Das SK, Choi SUS, Patel HE. Heat transfer in nanofluids - A review. Heat Transf Eng. 2006;27:3–19.
6. Kumar V, Sarkar J. Numerical and experimental investigations on heat transfer and pressure drop characteristics of Al_2O_3 -TiO_2 hybrid nanofluid in minichannel heat sink with different mixture ratio. Powder Technol. 2019;345:717–27. https://doi.org/10.1016/j.powtec.2019.01.061.
7. Gong L, Kota K, Tao W, Joshi Y. Parametric numerical study of flow and heat transfer in microchannels with wavy walls. J Heat Transfer. 2011;133.
8. Ambreen T, Kim MH. Comparative assessment of numerical models for nanofluids' laminar forced convection in micro and mini channels. Int J Heat Mass Transf. 2017;115:513–23. https://doi.org/10.1016/j.ijheatmasstransfer.2017.08.046.
9. Klazly M, Bognar G. Heat transfer enhancement for nanofluid flows over a microscale backward-facing step. Alexandria Eng J. 2022;61:8161–76. https://doi.org/10.1016/j.aej.2022.01.008.
10. Borah A, Mehta SK, Pati S. Analysis of conjugate heat transfer for forced convective flow through wavy minichannel. Int J Numer Methods Heat Fluid Flow. 2023;33:174–203.
11. Vajravel LV, KuppusamySwaminathan S, Baskaran S, Kalpoondi SR. Experimental investigations on heat transfer in a new minichannel heat sink. Int J Therm Sci. 2019;140:144–53. https://doi.org/10.1016/j.ijthermalsci.2019.02.029.
12. Balaji T, Rajendiran S, Selvam C, Lal DM. Enhanced heat transfer characteristics of water based hybrid nanofluids with graphene nanoplatelets and multi walled carbon nanotubes. Powder Technol. 2021;394:1141–57. https://doi.org/10.1016/j.powtec.2021.09.014.
13. Usman M, Hafiz S, Ali M, Sufyan A, Rashid D, Ullah S. Experimental investigation of TiO_2 – water nanofluid flow and heat transfer inside wavy mini-channel heat sinks. J Therm Anal Calorim. 2019;137:1279–94. https://doi.org/10.1007/s10973-019-08043-9.
14. Nivedita N, Ligrani P, Papautsky I. Dean flow dynamics in low-aspect ratio spiral microchannels. Sci Rep. 2017;7:1–10.
15. Lin L, Zhao J, Lu G, Wang XD, Yan WM. Heat transfer enhancement in microchannel heat sink by wavy channel with changing wavelength/amplitude. Int J Therm Sci. 2017;118:423–34. https://doi.org/10.1016/j.ijthermalsci.2017.05.013.
16. Xie G, Chen Z, Sunden B, Zhang W. Numerical predictions of the flow and thermal performance of water-cooled single-layer and double-layer wavy microchannel heat sinks. Numer Heat Transf Part A Appl. 2013;63:201–25.
17. Khoshvaght-Aliabadi M, Abbaszadeh A, Rashidi MM. Comparison of Co- and counter-current modes of operation for wavy minichannel heat sinks (WMHSs). Int J Therm Sci. 2022;171:107189. https://doi.org/10.1016/j.ijthermalsci.2021.107189.
18. Tariq HA, Anwar M, Muhammad H, Jamal A. Effect of dual flow arrangements on the performance of mini - channel heat sink : numerical study. J Therm Anal Calorim. 2021;143:2011–27. https://doi.org/10.1007/s10973-020-09617-8.
19. Ghasemi SE, Ranjbar AA, Hosseini MJ. Thermal and hydrodynamic characteristics of water-based suspensions of Al_2O_3 nanoparticles in a novel minichannel heat sink. J Mol Liq. 2017;230:550–6. https://doi.org/10.1016/j.molliq.2017.01.070.
20. Nanda Kishore PVR, Venkatachalapathy S, Kalidoss P. Experimental investigation on thermohydraulic performance of hybrid nanofluids in a novel minichannel heat sink. Thermochim Acta. 2023;721:179452.
21. Wang L, Luo X, Zhang J. Numerical study and performance analyses of counter flow minichannel heat sink with slots on ribs. Therm Sci Eng Prog. 2023;45:102116. https://doi.org/10.1016/j.tsep.2023.102116.
22. Hosseinirad E, Hormozi F. Thermal performance enhancement in a miniature channel using different passive methods. J Therm Anal Calorim. 2019;135:1849–61. https://doi.org/10.1007/s10973-018-7650-8.
23. Dominic A, Sarangan J, Suresh S, Devahdhanush VS. An experimental study of heat transfer and pressure drop characteristics of divergent wavy minichannels using nanofluids. Heat Mass Transf und Stoffuebertragung. 2017;53:959–71.
24. Sajid MU, Ali HM, Sufyan A, Rashid D, Zahid SU, Rehman WU. Experimental investigation of TiO_2–water nanofluid flow and heat transfer inside wavy mini-channel heat sinks. J Therm Anal Calorim. 2019;137:1279–94.
25. Xia GD, Liu R, Wang J, Du M. The characteristics of convective heat transfer in microchannel heat sinks using Al_2O_3 and TiO_2 nanofluids. Int Commun Heat Mass Transf. 2016;76:256–64.
26. Webb RL. Principles of enhanced heat transfer. 1994.
27. Saadoon ZH, Ali FH, Hamzah HK, Abed AM, Hatami M. Improving the performance of mini-channel heat sink by using wavy channel and different types of nanofluids. Sci Rep. 2022;12:9402. https://doi.org/10.1038/s41598-022-13519-0.
28. Ghaedamini H, Lee PS, Teo CJ. Developing forced convection in converging-diverging microchannels. Int J Heat Mass Transf. 2013;65:491–9. https://doi.org/10.1016/j.ijheatmasstransfer.2013.06.036.
29. Liu X, Yu J. Numerical study on performances of minichannel heat sinks with non-uniform inlets. Appl Therm Eng. 2016;93:856–64. https://doi.org/10.1016/j.applthermaleng.2015.09.032.
30. Standard A. ASHRAE Handbook 2009 Fundamentals (SI Edition). Ashrae Stand. 2009;24–5.
31. Chiam HW, Azmi WH, Usri NA, Mamat R, Adam NM. Thermal conductivity and viscosity of Al_2O_3 nanofluids for different based ratio of water and ethylene glycol mixture. Exp Therm Fluid Sci.

2017;81:420–9. https://doi.org/10.1016/j.expthermflusci.2016.09.013.

32. Ansari MQ, Zhou G. Influence of structured surface roughness peaks on flow and heat transfer performances of micro- and mini-channels. Int Commun Heat Mass Transf. 2020;110:104428.